

Chiral d -wave Superconductivity in a Triangular Surface Lattice Mediated by Long-range Interaction

Xiaodong Cao,¹ Thomas Ayrat,^{2,3} Zhicheng Zhong,^{1,4} Olivier Parcollet,³ Dirk Manske,¹ and Philipp Hansmann^{1,5}

¹*Max-Planck-Institut für Festkörperforschung, Heisenbergstrasse 1, 70569 Stuttgart, Germany*

²*Physics and Astronomy Department, Rutgers University, Piscataway, NJ 08854, USA*

³*Institut de Physique Théorique (IPhT), CEA, CNRS, UMR 3681, 91191 Gif-sur-Yvette, France*

⁴*Ningbo Institute of Materials Technology and Engineering,
Chinese Academy of Sciences, 315201 Ningbo, China*

⁵*Institut für Theoretische Physik, Eberhard Karls Universität Tübingen, Auf der Morgenstelle 14, 72076 Tübingen*

(Dated: October 11, 2017)

Correlated ad-atom systems on the Si(111) surface have recently attracted an increased attention as strongly correlated systems with a rich phase diagram. We study these materials by a single band model on the triangular lattice including $1/r$ long-range interaction. Employing the recently proposed TRILEX method we find an unconventional superconducting phase of chiral d -wave symmetry in hole-doped systems. The superconductivity is driven simultaneously by both charge and spin fluctuations and is strongly enhanced by the long-range tail of the interaction. We provide an analysis of the relevant collective bosonic modes and explain how in triangular symmetry both charge and spin channels contribute to the Cooper pairing.

PACS numbers:

The search for materials with unconventional high temperature superconductivity (SC) has been one of the most active fields in correlated solid state physics since the discovery of the cuprate high T_c compounds. Sophisticated synthesis technology nowadays allows for the construction of new materials like heterostructures or surface systems on an atomic length scale. Recently, many-body studies on experimentally well controlled correlated ad-atom lattices X:Si(111) and X:Ge(111) with (X=Pb,Sn,C) led to interesting results[1–5] and allowed to unify the materials in a single phase diagram [3]. Due to sizable long-range interaction in the triangular lattice geometry, some of the materials were shown to be in close vicinity to a triple point between a Fermi liquid, a Mott insulator, and a charge-ordered insulator. Sn:Si(111) and Pb:Si(111) in particular turned out to be close to a charge-order Mott insulator phase transition with sizable charge fluctuations visible in core level spectroscopy [5] of Sn:Si(111). In complementary studies [4] the importance of spin fluctuations for Sn:Si(111) was emphasized. Such materials are, hence, promising candidates to search for new physics like unconventional superconductivity.

For such systems theoretical methods are needed which are capable to capture both local and non-local electronic correlations. Dynamical mean-field theory (DMFT) [6, 7] has been proven to be a powerful approach to treat local correlations and Mott physics. If non-local interactions have to be treated, extended DMFT (EDMFT) [8] captures their effects on the local self energy by a retarded onsite interaction. Local approximations like DMFT and EDMFT are, however, not sufficient when non-local fluctuations start to play an important role. To overcome these shortcomings of DMFT, several extensions have been proposed [9, 10]. Cluster extensions of DMFT in real and reciprocal space [10–13], e.g., are capable to

treat non-local short range fluctuations. Long range fluctuations, on the other hand, can be taken into account by DMFT+GW [14–16] or dual boson methods [17–20]. For our study we employ the recently developed TRILEX approximation [21–24] which combines a balanced treatment of long range spin and charge fluctuations with comparatively little computational effort.

In this letter we show that the triangular lattice model for the ad-atom materials has a dome shaped superconducting phase of chiral d -wave symmetry as a function of hole doping in realistic parameter regimes. The long-range interaction is key for enhanced critical temperatures and distinguishes the ad-atom Hamiltonian from triangular Hubbard models [25–32]. By analyzing spin- and charge response functions we further show that the pairing mechanism crosses over from a cumulative spin/charge fluctuation character at small dopings to a charge dominated one at large doping.

The low energy Hamiltonian on the triangular lattice with long-range interaction reads:

$$H = \sum_{i,j,\sigma} t_{ij} \hat{c}_{i\sigma}^\dagger \hat{c}_{j\sigma} + \frac{1}{2} \sum_{i,j} U_{ij} \hat{n}_i \hat{n}_j - \mu \sum_i \hat{n}_i, \quad (1)$$

where $\hat{c}_{i\sigma}^\dagger$ ($\hat{c}_{i\sigma}$) are electron creation (annihilation) operators on site i with spin $\sigma = \uparrow, \downarrow$. $\hat{n}_i = \hat{n}_{i\uparrow} + \hat{n}_{i\downarrow}$ is the density operator on site i , and μ is the chemical potential. t_{ij} and U_{ij} are the hopping integrals and long-range Coulomb interaction strength between sites i and j . For translational invariant two-dimensional systems, the long-range Coulomb interaction, in momentum space, reads $U_{\mathbf{q}} = U_0 + V \sum_{i \neq 0} e^{i\mathbf{q} \cdot \mathbf{R}_i} / |\mathbf{R}_i|$ where \mathbf{R}_i are real space coordinates, U_0 is the on-site interaction, and V is the strength of the long-range interaction respectively (Suppl. Mat. A). More specifically, we adopt hopping

parameters up to next-nearest-neighbors ($t = 0.042\text{eV}$ and $t' = -0.02\text{eV}$) from [2, 3] derived from density functional theory (DFT) for the Pb:Si(111) ad-atom system (closest to the triple point) and vary the interaction parameters in realistic regimes for the ad-atom materials found by constrained random phase approximation [3].

TRILEX approximates the three-legged fermion-boson interaction vertex using a local self-consistent quantum impurity model. For systems retaining SU(2) symmetry, the self-consistent TRILEX equations [21–24] for the fermionic single particle self-energy $\Sigma(\mathbf{k}, i\omega_n)$ and bosonic polarization in charge and spin channel $P^{c,s}(\mathbf{q}, i\nu_n)$ can be rewritten as:

$$\begin{aligned}\Sigma_{\mathbf{k}, i\omega_n} &= \Sigma_{i\omega_n}^{\text{imp}} - \sum_{\eta, \mathbf{q}, i\nu_n} m^\eta \tilde{G}_{\mathbf{k}+\mathbf{q}, i\omega_n+i\nu_n} \tilde{W}_{\mathbf{q}, i\nu_n}^\eta \Lambda_{i\omega_n, i\nu_n}^{\text{imp}, \eta} \\ P_{\mathbf{q}, i\nu_n}^\eta &= P_{i\nu_n}^{\text{imp}, \eta} + 2 \sum_{\mathbf{k}, i\omega_n} \tilde{G}_{\mathbf{k}+\mathbf{q}, i\omega_n+i\nu_n} \tilde{G}_{\mathbf{k}, i\omega_n} \Lambda_{i\omega_n, i\nu_n}^{\text{imp}, \eta}\end{aligned}\quad (2)$$

where the index $\eta = \{c, s\}$ corresponds to charge and spin channel respectively, and ω_n and ν_n are fermionic and bosonic Matsubara frequencies. $G_{\mathbf{k}, i\omega_n}$ is the dressed Green's function, and $W_{\mathbf{q}, i\nu_n}^{c,s}$ are the fully screened interactions in the charge and spin channel respectively. The local part of self-energy and polarization are replaced by their impurity counterparts $\Sigma_{i\omega_n}^{\text{imp}}$ and $P_{i\nu_n}^{\text{imp}, \eta}$ respectively, and for any quantity X , $\tilde{X}_{\mathbf{k}, i\omega_n} = X_{\mathbf{k}, i\omega_n} - X_{i\omega_n}^{\text{loc}}$ with $X_{i\omega_n}^{\text{loc}} = \frac{1}{N_k} \sum_{\mathbf{k} \in \text{B.Z.}} X_{\mathbf{k}, i\omega_n}$. We employ the Heisenberg decomposition of the interaction [22], for which we have $m_c = 1$, $m_s = 3$ and $W_{\mathbf{q}, i\nu_n}^\eta = U_{\mathbf{q}}^\eta [1 - U_{\mathbf{q}}^\eta P_{\mathbf{q}, i\nu_n}^\eta]^{-1}$. Bare interactions in charge and spin channel are, hence, given by $U_{\mathbf{q}}^c = \frac{U_0}{2} + v_{\mathbf{q}}$ and $U_{\mathbf{q}}^s = -\frac{U_0}{6}$. This spin/charge ratio is a choice (dubbed “Fierz ambiguity” [22, 24]). Moreover, in the parameter range explored in this paper we have observed (Fig. 2 and Suppl. Mat. B) that using $\Lambda_{i\omega_n, i\nu_n}^{\text{imp}, \eta} \approx 1$ in Eq. (2) does not change our results qualitatively as it was also found in [23]. This simplified TRILEX version can be seen as a GW+EDMFT like scheme which, however, can treat simultaneously both charge and spin fluctuations. The impurity problem was solved using the segment picture in the hybridization-expansion continuous time quantum Monte-Carlo algorithm [33–37] implemented with the TRIQS library [38].

In order to probe superconductivity instabilities, we solve the linearized gap equation with converged simplified TRILEX results as an input [23]. For singlet d -wave pairing the corresponding eigenvalue equation for the gap reads

$$\lambda \Delta_{\mathbf{k}, i\omega_n} = - \sum_{\mathbf{k}', i\omega'_n} |G_{\mathbf{k}', i\omega'_n}|^2 \Delta_{\mathbf{k}', i\omega'_n} V_{\mathbf{k}-\mathbf{k}', i\omega_n-i\omega'_n}^{\text{eff}}, \quad (3)$$

where the singlet pairing interaction is given by

$$V_{\mathbf{q}, i\nu_n}^{\text{eff}} = m^c W_{\mathbf{q}, i\nu_n}^c - m^s W_{\mathbf{q}, i\nu_n}^s \quad (4)$$

and is therefore a combination of effective interaction in charge and spin channel. The SC instability occurs when

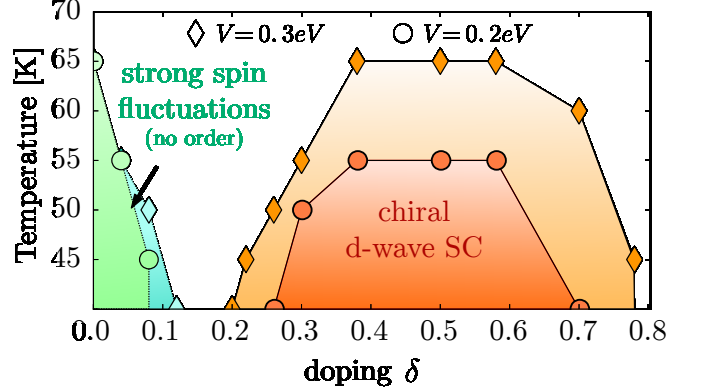


FIG. 1: Phase diagram of the Hamiltonian (1) as function of temperature (for $T > 40\text{K}$) and doping for $U_0 = 0.7\text{eV}$, $V = 0.2\text{eV}$ (circles) and $V = 0.3\text{eV}$ (diamonds). Green/blue regions correspond to $1 \geq \text{Max}[-P^s(\mathbf{q}, i\nu_n = 0)U^s] \geq 0.95$ for $\mathbf{q} \in \text{B.Z.}$. Orange/red regions indicate chiral d -wave superconductivity.

the largest eigenvalue $\lambda = 1$. The pairing symmetry is monitored by the \mathbf{k} dependence of the gap function $\Delta_{\mathbf{k}, i\omega_n}$.

Emergence of d-wave superconductivity – In Fig. 1 we plot the temperature–doping (T – δ) phase diagram for $V = 0.2\text{eV}$ and $V = 0.3\text{eV}$ for a fixed value of $U_0 = 0.7\text{eV}$ in the simplified TRILEX approximation. At half-filling ($\delta = 0$) we obtain a correlated Fermi liquid (Suppl. Mat. C) with strong magnetic fluctuations. The static spin-spin correlation function $\chi^s(\mathbf{q}, i\nu_n = 0)$ is very large at some \mathbf{q} but has not diverged yet, i.e. no phase transition has occurred. More precisely, we use $\text{Max}[-P^s(\mathbf{q}, i\nu_n = 0)U^s]$ with $\mathbf{q} \in \text{B.Z.}$ which reaches 1 at a second order spin ordering phase transition to quantify the strength of the spin fluctuations and color code regions in the phase diagram for which $1 > \text{Max}[-P^s(\mathbf{q}, i\nu_n = 0)U^s] \geq 0.95$ in green ($V = 0.2\text{eV}$) and blue ($V = 0.3\text{eV}$). From this plot we see that spin fluctuations are slightly enhanced by increasing V . For $\delta > 0.2$ we observe the emergence of a dome-shaped superconducting phase (a plot of the λ parameter in Eq. (3) as a function of temperature is shown in the Suppl. Mat. D). The pairing symmetry of the SC phase is of d -wave character and includes doubly degenerate $d_{x^2-y^2}$ - and d_{xy} -wave pairing channels (see Suppl. Mat. E for a plot of the gap function). The degeneracy of these two pairing symmetries is protected by the C_{6v} point group of the triangular lattice, which then yields chiral d -wave symmetry below T_c to maximize condensation energy. The predicted chiral SC phase depends crucially on V : T_c increases from $V = 0.2\text{eV}$ (red circles) to $V = 0.3\text{eV}$ (orange diamonds) as shown in Fig. 1. Moreover, for $V = 0.0\text{eV}$ and $V = 0.1\text{eV}$ (not shown here) we do not find a SC phase for $T > 40\text{K}$.

Impact of long-range interaction on susceptibilities and

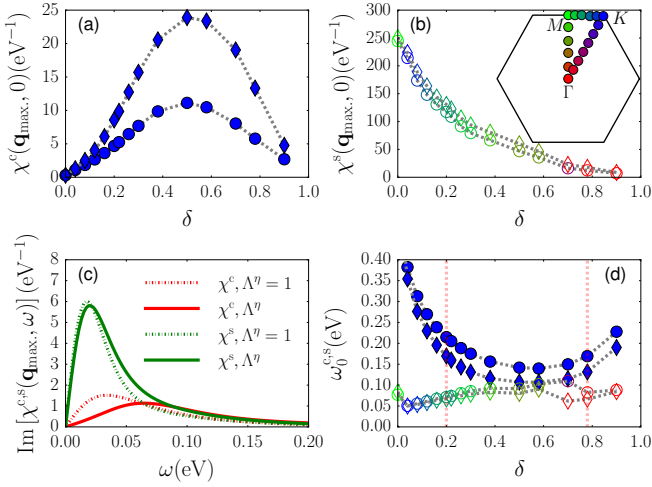


FIG. 2: Maximum values of the static charge (a) and spin (b) response functions versus hole doping. Color coding indicates the position of the maximum in the first Brillouin zone as defined in the inset. Data is shown for fixed $U_0 = 0.7\text{eV}$ and $T = 40\text{K}$ and non-local interaction strength $V = 0.3\text{eV}$ (diamonds) and $V = 0.2\text{eV}$ (circles); (c) Charge- and spin response functions on the real frequency axis (obtained by analytical continuation with the maximum entropy method[39]) at their maximum in momentum space ($\mathbf{q}_{\text{max.}}$) with (dashed) and without (solid) vertex corrections for $T = 116\text{K}$ and $\delta = 0.2$; (d) Characteristic frequency of charge- (filled symbols) and spin (open symbols) fluctuations with the same convention and parameters as (a) and (b).

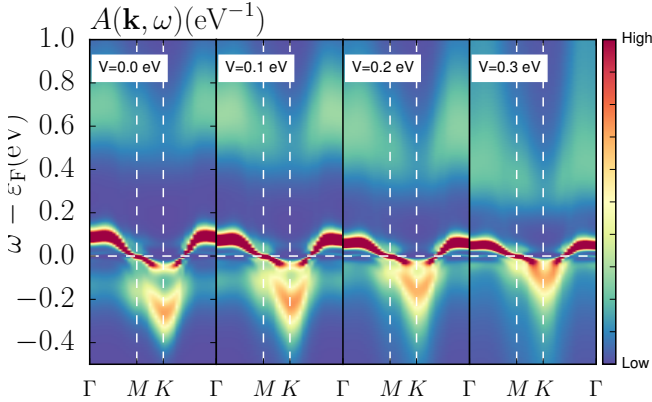


FIG. 3: Single particle spectral function $A(\mathbf{k}, \omega)$ along the path Γ -M-K- Γ (see inset of Fig. 2) for fixed doping $\delta = 0.2$, $T = 40\text{K}$, $U_0 = 0.7\text{eV}$ and four values of V .

single particle spectra – The impact of V on the SC instability is reflected in the effective singlet-pairing interaction $V_{\mathbf{q}, i\nu_n}^{\text{eff}}$ which depends on fluctuations in *both* charge and spin channels. We analyze the respective susceptibilities $\chi^{c/s}(\mathbf{q}, i\nu_n)$ with the data shown in Fig. 2: In the upper panels we show the maximum values of the static ($i\nu_n = 0$) charge (left hand side) and spin (right hand side) susceptibilities as a function of hole doping.

The corresponding position of the maximum in the first Brillouin zone is color coded (see inset).

The charge fluctuations increase with hole doping to a maximum value around $\delta = 0.5$ and, thereafter, decrease approaching the “empty” limit at $\delta = 1$. The spin fluctuations, instead, decrease monotonically as a function of δ . While $\chi^c(\mathbf{q}, i\nu_n = 0)$ always peaks at K , the maximum of $\chi^s(\mathbf{q}, i\nu_n = 0)$ moves from M to K when the system is slightly doped, and then follows $K \rightarrow M \rightarrow \Gamma$ when the system is further hole-doped. The peak position of the charge response function as a function of doping remains at the K point since its momentum dependence is mainly determined by the doping independent $v(\mathbf{q})$ which energetically favors a 3×3 charge configuration in real space [3]. The momentum dependence of the spin response function, however, is mostly determined by the topology of the Fermi surface. Indeed, the V dependence is much stronger for the charge response (compare diamond ($V = 0.3\text{eV}$) and circle ($V = 0.2\text{eV}$) symbols in Fig. 2). There are, however, small effects of V to the spin response function which can be understood by the V -dependent renormalization of the one-particle spectra as show in Fig. 3 [40]. At fixed $T = 40\text{K}$ and $\delta = 0.2$, V is increased from 0.0eV to 0.3eV (subplots from left to right hand side). Upon increasing V , the bandwidth is effectively reduced and the spectral weight near to the Fermi energy is increased. Consequently, particle-hole excitations that contribute to the spin polarization $P^s(\mathbf{q}, i\nu_n)$ and the spin susceptibility are enhanced.

We now extend these considerations to the frequency dependence of the bosonic fluctuations. In Fig. 2c we plot the dynamic response functions at the \mathbf{q} -points where they are maximal ($\mathbf{q}_{\text{max.}}$) for doping $\delta = 0.2$. The data clearly shows a peaked structure of the dynamic response functions. Moreover, we show in this plot the impact of the vertex corrections (compare solid and dashed lines) which are only quantitative in the considered case as claimed in the introduction. Fig. 2d shows the doping dependence of the characteristic frequency $\omega_0^{c,s}(\mathbf{q}_{\text{max.}})$ defined by $\omega_0^{c,s}(\mathbf{q}_{\text{max.}}) = \int_0^\infty \omega \text{Im}[\chi^{c,s}(\mathbf{q}_{\text{max.}}, \omega)] d\omega / \int_0^\infty \text{Im}[\chi^{c,s}(\mathbf{q}_{\text{max.}}, \omega)] d\omega$ in both channels. Inside the superconducting region (indicated by the vertical red dashed lines) the characteristic frequency of the fluctuations are of the order of $100 - 200\text{meV}$. Moreover, $|\omega_0^c - \omega_0^s|$ is small and minimal for the region of maximum T_c . In agreement with our discussion above we see that an increase of V yields even smaller $|\omega_0^c - \omega_0^s|$ which suggests that charge and spin contributions to the SC pairing mechanism are cumulative.

Separating spin and charge channels in the pairing mechanism – In order to disentangle the interplay between charge and spin degrees of freedom in gap equation (3), we solve for λ including contributions from only spin- (λ_s) and only charge channel (λ_c), i.e., $V_{\mathbf{q}, i\nu_n}^{\text{eff}} = -3W_{\mathbf{q}, i\nu_n}^s$ and $V_{\mathbf{q}, i\nu_n}^{\text{eff}} = W_{\mathbf{q}, i\nu_n}^c$ respectively. First, we follow the phase boundary of the SC phase in the under-

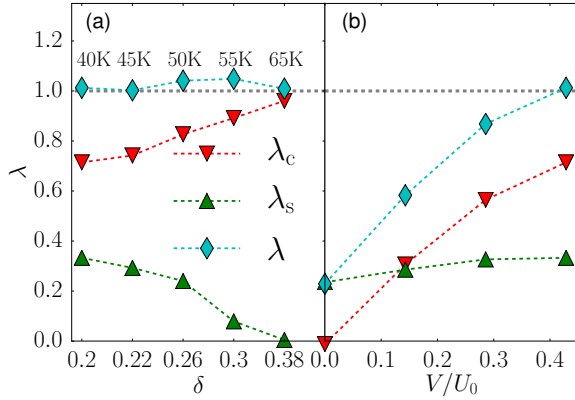


FIG. 4: Eigenvalue λ of the gap equation Eq. (3) ($\lambda = 1$ signals SC transition) for full effective singlet pairing interaction $V_{\mathbf{q},i\nu_n}^{\text{eff}}$ (cyan) and charge/spin only channels (red/green). (a) Plot for $V = 0.3\text{eV}$ along the SC phase boundary up to doping $\delta = 0.38$. (b) Plot as a function of V for fixed doping $\delta = 0.2$ and temperature $T = 40\text{K}$.

doped regime for fixed $V = 0.3\text{eV}$ starting from $(\delta, T) = (0.2, 40\text{K})$ up to $(\delta, T) = (0.38, 65\text{K})$. In Fig. 4(a) we plot λ , λ_s , and λ_c : Since we are following the phase transition line, $\lambda \approx 1$. λ_c and λ_s are both smaller than λ and $\lambda_c + \lambda_s \approx \lambda$ indicating a cumulative charge and spin contribution for the chiral d -wave pairing in the underdoped regime. The same conclusion can be drawn when the λ values are calculated at the critical doping $\delta_c = 0.2$ as a function of the non-local interaction V as depicted in Fig. 4(b).

Our data indicates that overall both spin- and charge fluctuations are important for the SC phase. As a function of doping, however, we observe that charge fluctuations become increasingly dominant and λ_s becomes negligible. This effect is reflected in the V dependence of the SC dome in Fig. 1 which is stronger at larger dopings. We arrive at the same conclusions when we analyze the dependence of λ on the choice of the Fierz parameter that defines the charge-to-spin fluctuation ratio (Suppl. Mat. F).

Let us stress two important points: i) The true long-range character is crucial in our range of parameters. If only short-range (i.e. nearest-neighbor) interactions are considered charge ordering is overestimated and long before any SC emerges the system turns into a charge ordered insulator as proven by calculations shown in the Suppl. Mat. G. ii) The degeneracy of $d_{x^2-y^2}$ - and d_{xy} -wave pairing state is important for the cumulative charge and spin interplay. Since the origin of this degeneracy is connected to the lattice symmetry group, a different behavior can be expected for the 2D square lattice (see Suppl. Mat. H): in the square geometry with relatively large V/U_0 , the \mathbf{q} dependence of $\chi^c(\mathbf{q}, i\nu_n = 0)$ favors d_{xy} -pairing symmetry while $\chi^s(\mathbf{q}, i\nu_n = 0)$ prefers $d_{x^2-y^2}$ -pairing symmetry, and the two channels compete with each other.

In conclusion we predict the existence of a dome shaped unconventional chiral d -wave superconducting phase for hole-doped triangular lattice systems with $\propto 1/r$ interactions which could be realized by hole-doping existing α phase Si(111) ad-atom materials. The analysis of spin and charge correlation functions reveals that lattice geometry as well as the non-local interaction are necessary conditions for the emergence of superconductivity. The nature of the pairing undergoes a crossover from a combined charge/spin mechanism in the underdoped regime towards a charge fluctuation dominated one at higher doping. In future studies high hole-doping levels will be considered in more detail. Here, triplet f -wave pairing symmetry may begin to become important due to the appearance of a disconnected Fermi surface [41].

A. Acknowledgments

OP and TA are supported by the FP7/ERC, under Grant Agreement No. 278472-MottMetals. We thank Yi Lu, Alessandro Toschi, Ciro Taranto and Thomas Schaefer, Daniil Mantadakis for helpful discussions.

-
- [1] S. Schuwalow, D. Grieger, and F. Lechermann, Phys. Rev. B **82**, 035116 (2010), URL <http://link.aps.org/doi/10.1103/PhysRevB.82.035116>.
 - [2] P. Hansmann, L. Vaugier, H. Jiang, and S. Biermann, Journal of Physics: Condensed Matter **25**, 094005 (2013), URL <http://stacks.iop.org/0953-8984/25/i=9/a=094005>.
 - [3] P. Hansmann, T. Ayral, L. Vaugier, P. Werner, and S. Biermann, Phys. Rev. Lett. **110**, 166401 (2013), URL <http://link.aps.org/doi/10.1103/PhysRevLett.110.166401>.
 - [4] G. Li, P. Höpfner, J. Schäfer, C. Blumenstein, S. Meyer, A. Bostwick, E. Rotenberg, R. Claessen, and W. Hanke, Nature communications **4**, 1620 (2013).
 - [5] P. Hansmann, T. Ayral, A. Tejada, and S. Biermann, Scientific reports **6** (2016).
 - [6] A. Georges, G. Kotliar, W. Krauth, and M. J. Rozenberg, Rev. Mod. Phys. **68**, 13 (1996), URL <https://link.aps.org/doi/10.1103/RevModPhys.68.13>.
 - [7] G. Kotliar, S. Y. Savrasov, K. Haule, V. S. Oudovenko, O. Parcollet, and C. A. Marianetti, Rev. Mod. Phys. **78**, 865 (2006), URL <https://link.aps.org/doi/10.1103/RevModPhys.78.865>.
 - [8] Q. Si and J. L. Smith, Phys. Rev. Lett. **77**, 3391 (1996), URL <http://link.aps.org/doi/10.1103/PhysRevLett.77.3391>.

- [9] G. Rohringer, H. Hafermann, A. Toschi, A. Katanin, A. Antipov, M. Katsnelson, A. Lichtenstein, A. Rubtsov, and K. Held, arXiv preprint arXiv:1705.00024 (2017).
- [10] T. A. Maier, M. Jarrell, T. Pruschke, and M. H. Hettler, Reviews of Modern Physics **77**, 1027 (2005), ISSN 00346861.
- [11] M. H. Hettler, A. N. Tahvildar-Zadeh, M. Jarrell, T. Pruschke, and H. R. Krishnamurthy, Physical Review B **58**, R7475 (1998), ISSN 0163-1829, URL <http://arxiv.org/abs/cond-mat/9803295>.
- [12] A. I. Lichtenstein and M. I. Katsnelson, Physical Review B **62**, R9283 (2000), ISSN 0163-1829.
- [13] G. Kotliar, S. Y. Savrasov, G. Pálsson, and G. Biroli, Phys. Rev. Lett. **87**, 186401 (2001), URL <https://link.aps.org/doi/10.1103/PhysRevLett.87.186401>.
- [14] P. Sun and G. Kotliar, Phys. Rev. B **66**, 085120 (2002), URL <http://link.aps.org/doi/10.1103/PhysRevB.66.085120>.
- [15] P. Sun and G. Kotliar, Phys. Rev. Lett. **92**, 196402 (2004), URL <http://link.aps.org/doi/10.1103/PhysRevLett.92.196402>.
- [16] T. Ayral, S. Biermann, and P. Werner, Phys. Rev. B **87**, 125149 (2013), URL <http://link.aps.org/doi/10.1103/PhysRevB.87.125149>.
- [17] A. Rubtsov, M. Katsnelson, and A. Lichtenstein, Annals of Physics **327**, 1320 (2012), ISSN 0003-4916, URL <http://www.sciencedirect.com/science/article/pii/S0003491612000164>.
- [18] E. G. C. P. van Loon, H. Hafermann, A. I. Lichtenstein, A. N. Rubtsov, and M. I. Katsnelson, Phys. Rev. Lett. **113**, 246407 (2014), URL <http://link.aps.org/doi/10.1103/PhysRevLett.113.246407>.
- [19] E. G. C. P. van Loon, M. Schüller, M. I. Katsnelson, and T. O. Wehling, Phys. Rev. B **94**, 165141 (2016), URL <http://link.aps.org/doi/10.1103/PhysRevB.94.165141>.
- [20] H. Hafermann, E. G. C. P. van Loon, M. I. Katsnelson, A. I. Lichtenstein, and O. Parcollet, Phys. Rev. B **90**, 235105 (2014), URL <http://link.aps.org/doi/10.1103/PhysRevB.90.235105>.
- [21] T. Ayral and O. Parcollet, Phys. Rev. B **92**, 115109 (2015), URL <http://link.aps.org/doi/10.1103/PhysRevB.92.115109>.
- [22] T. Ayral and O. Parcollet, Phys. Rev. B **93**, 235124 (2016), URL <http://link.aps.org/doi/10.1103/PhysRevB.93.235124>.
- [23] J. Vucicevic, T. Ayral, and O. Parcollet, Phys. Rev. B **96**, 104504 (2017).
- [24] T. Ayral, J. Vucicevic, and O. Parcollet, arXiv preprint arXiv:1706.01388 (2017).
- [25] S. Zhou and Z. Wang, Phys. Rev. Lett. **100**, 217002 (2008), URL <https://link.aps.org/doi/10.1103/PhysRevLett.100.217002>.
- [26] S.-Q. Su, Z.-B. Huang, R. Fan, and H.-Q. Lin, Phys. Rev. B **77**, 125114 (2008), URL <https://link.aps.org/doi/10.1103/PhysRevB.77.125114>.
- [27] K. Kuroki, Phys. Rev. B **81**, 104502 (2010), URL <https://link.aps.org/doi/10.1103/PhysRevB.81.104502>.
- [28] R. Nandkishore, L. Levitov, and A. Chubukov, Nature Physics **8**, 158 (2012).
- [29] K. S. Chen, Z. Y. Meng, U. Yu, S. Yang, M. Jarrell, and J. Moreno, Phys. Rev. B **88**, 041103 (2013), URL <http://link.aps.org/doi/10.1103/PhysRevB.88.041103>.
- [30] M. L. Kiesel, C. Platt, W. Hanke, D. A. Abanin, and R. Thomale, Phys. Rev. B **86**, 020507 (2012), URL <https://link.aps.org/doi/10.1103/PhysRevB.86.020507>.
- [31] M. L. Kiesel, C. Platt, W. Hanke, and R. Thomale, Phys. Rev. Lett. **111**, 097001 (2013), URL <https://link.aps.org/doi/10.1103/PhysRevLett.111.097001>.
- [32] A. M. Black-Schaffer, W. Wu, and K. Le Hur, Phys. Rev. B **90**, 054521 (2014), URL <https://link.aps.org/doi/10.1103/PhysRevB.90.054521>.
- [33] P. Werner, A. Comanac, L. de' Medici, M. Troyer, and A. J. Millis, Phys. Rev. Lett. **97**, 076405 (2006), URL <https://link.aps.org/doi/10.1103/PhysRevLett.97.076405>.
- [34] T. Ayral, P. Werner, and S. Biermann, Phys. Rev. Lett. **109**, 226401 (2012), URL <https://link.aps.org/doi/10.1103/PhysRevLett.109.226401>.
- [35] P. Werner and A. J. Millis, Phys. Rev. Lett. **99**, 146404 (2007), URL <https://link.aps.org/doi/10.1103/PhysRevLett.99.146404>.
- [36] J. Otsuki, Phys. Rev. B **87**, 125102 (2013), URL <https://link.aps.org/doi/10.1103/PhysRevB.87.125102>.
- [37] H. Hafermann, Phys. Rev. B **89**, 235128 (2014), URL <https://link.aps.org/doi/10.1103/PhysRevB.89.235128>.
- [38] O. Parcollet, M. Ferrero, T. Ayral, H. Hafermann, I. Krivenko, L. Messio, and P. Seth, Computer Physics Communications **196**, 398 (2015), ISSN 0010-4655, URL <http://www.sciencedirect.com/science/article/pii/S0010465515001666>.
- [39] M. Jarrell and J. Gubernatis, Physics Reports **269**, 133 (1996), ISSN 0370-1573, URL <http://www.sciencedirect.com/science/article/pii/0370157395000747>.
- [40] P. Werner and M. Casula, Journal of Physics: Condensed Matter **28**, 383001 (2016), URL <http://stacks.iop.org/0953-8984/28/i=38/a=383001>.
- [41] K. Kuroki and R. Arita, Phys. Rev. B **63**, 174507 (2001), URL <https://link.aps.org/doi/10.1103/PhysRevB.63.174507>.

Supplemental Material

Appendix A: Formulation of the non-local interaction $v(\mathbf{q})$ in the lattice model

The long-range interaction in momentum space can be formulated as:

$$U(\mathbf{q}) = U_0 + v(\mathbf{q}) = U_0 + V \sum_{i \neq 0} \frac{1}{|\mathbf{R}_i|/a} e^{i\mathbf{q} \cdot \mathbf{R}_i}, \quad (\text{A1})$$

where a is the lattice constant. In order to tackle the convergence problem given by a Madelung like lattice-sum we follow the ideas of Ewald and rewrite the sum in terms of a short-range contribution and a long-range contribution. The long-range contribution can be obtained analytically, while the short-range contribution is calculated numerically with a parameter η controlling the summation range:

$$v(\mathbf{q}) = V \left(\sum_{\substack{\mathbf{R} \in \text{BL} \setminus \{0\} \\ |\mathbf{R}| < N}} \frac{\text{erfc}(|\mathbf{R}|/\eta)}{|\mathbf{R}|} e^{i\mathbf{q} \cdot \mathbf{R}} + \frac{2\pi}{|\mathbf{q}|} \text{erfc}\left(\frac{|\mathbf{q}|\eta}{2}\right) - \frac{1}{\eta} \frac{2}{\sqrt{\pi}} \right), \quad (\text{A2})$$

where $\sqrt{N} \ll \eta \lesssim N$ and N is the linear size of the lattice ($N = 64$ in our calculations). Here we have taken the nearest-neighbor distance $a = 1$. The function $\text{erfc}(x)$ is the complementary of the error function $\text{erf}(x)$, namely $\text{erfc}(x) = 1 - \text{erf}(x)$. BL represents sites in the Bravais lattice.

Appendix B: Effects of the vertex $\Lambda^{\text{imp},\eta}(i\omega_n, \nu_n)$

Upon increasing the long-range interaction strength from $V = 0.1\text{eV}$ to $V = 0.3\text{eV}$, the static charge- and spin response functions are enhanced (see Fig. 5 (a) and (b)). Simultaneously, their characteristic frequencies are shifted to lower energies shown in Fig. 5 (c) and (d) (note that the data for the dynamic response for $V = 0.3\text{ eV}$ is shown in the main text figure 2(c)). Hence, our conclusions about the V dependence is not compromised by vertex corrections. In Fig. 5(a) we see that $\Lambda^{\text{imp},c}(i\omega_n, i\nu_n)$ partially suppresses the charge response function. I.e., the critical nearest-neighbor interaction strength V_c of metal to charge-ordered phase transition is shifted to larger values if the three-legged vertex is taken into account. For the spin response function (Fig. 5(b)), $\Lambda^{\text{imp},s}(i\omega_n, i\nu_n)$ slightly suppresses its value and shifts its maximum closer to M . Finally, the λ values obtained from the solution of the gap equation for $V = 0.3\text{eV}$ are actually *increased* from 0.49 to 0.52 as a consequence of the vertex corrections (for $V = 0.1\text{eV}$ λ increases from 0.271 to 0.274). This means that inclusion of vertex corrections leads to even higher values of T_c which was found also in another recent TRILEX study for the 2D square lattice Hubbard model [23].

Appendix C: $\text{Im}[\Sigma_{\text{loc}}(i\omega_n)]$ at different doping levels

The Fermi liquid character of the normal state above the critical temperature can be seen from the imaginary part of the local fermionic self energy on the Matsubara axis. In Fig. 6 we show $\text{Im}[\Sigma_{\text{loc}}(i\omega_n)]$ for different doping levels. From the data shown we can estimate the mass enhancement of the correlated quasiparticles $m/m^* = [1 - \text{Im}[\Sigma_{\text{loc}}(i\omega_0)]/\omega_0]^{-1} = 0.047, 0.21, 0.38$ corresponding to $\delta = 0.0, 0.2, 0.5$ respectively.

Appendix D: Temperature dependence of λ

In Fig. 7 we plot λ as a function of temperature for different doping levels. The SC instability is indicated by $\lambda = 1$ (for instance $\delta = 0.2$ at $T \approx 40\text{K}$ and $\delta = 0.26$ at $T \approx 55\text{K}$). Please note that no extrapolation of $\lambda(T)$ is needed due to the absence of a magnetically ordered phase, different from the square lattice case [23].

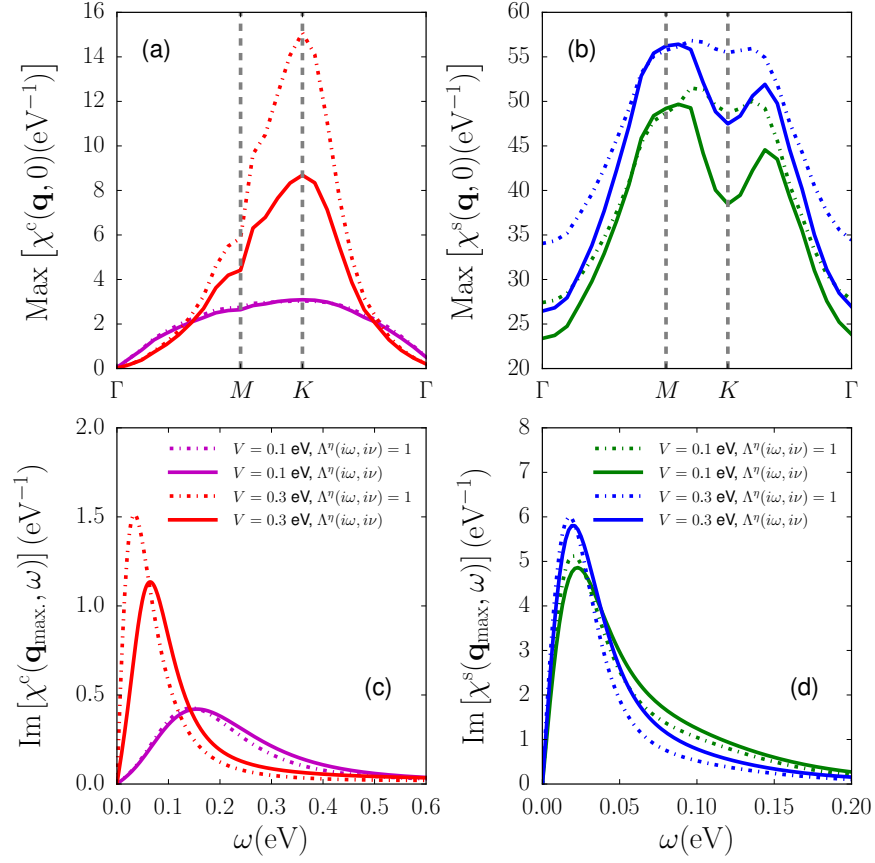


FIG. 5: Charge- and spin response functions with (solid lines) and without (dashed lines) vertex corrections for $V = 0.1\text{eV}$ and $V = 0.3\text{eV}$. Upper panels: Static charge- (a) and spin (b) response function along the high symmetry points. Lower panels: Spectrum of charge- (c) and spin (d) response function at $\mathbf{q} = \mathbf{q}_{\text{max}}$, with \mathbf{q}_{max} being the peak position of the corresponding static response function. The shown results were obtained for $U_0 = 0.7\text{eV}$, $T = 116\text{K}$ and $\delta = 0.2$.

Appendix E: Momentum dependence of chiral d -wave gap function

In Fig. 8 we plot the momentum dependence of the chiral d -wave gap function $\Delta_{d+id'}$ obtained from the solution of the gap equation (3) for the triangular lattice with long-range interaction. The chiral $d + id'$ superconducting state is a time-reversal symmetry breaking state with non-trivial topology as can be seen in Fig. 8(d) from the non-zero winding number(= 2) along the Fermi surface. This indicates the existence of two edge states.

Appendix F: Dependence on the charge to spin ratio

As mentioned in the main text, the ratio of the bare interaction in charge- and spin channels may be parametrized by α , i.e.,

$$U^c(\mathbf{q}) = (3\alpha - 1)U_0 + v(\mathbf{q}), U^s = (\alpha - 2/3)U_0 \quad (\text{F1})$$

for Heisenberg decoupling [21]. The TRILEX results depend a priori on the choice of the Fierz parameter α . In the following, we show that our conclusions are robust with respect to the choice of α . While there is a sizable dependence of the λ values on α , this dependency leads only to a quantitative shift of the boundary of the SC phase but SC is never suppressed.

Since α controls the contributions from charge- and spin fluctuations to the SC pairing glue, we can exploit the dependence of the results on α as an indicator of their respective role in the emergence of SC. As shown in Fig. 9, for comparatively small doping ($\delta \sim 0.2$) λ is increased by decreasing α (i.e. emphasizing spin fluctuations). This indicates that at small doping spin fluctuations are the main contributor to the emergence of superconductivity. At

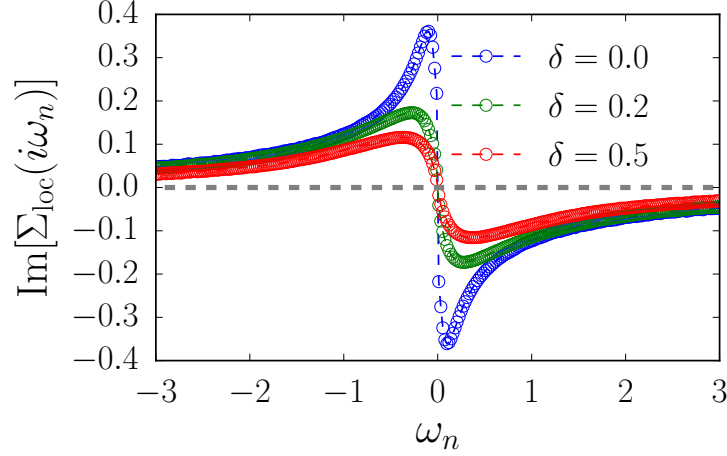


FIG. 6: Plot of the imaginary part of the local fermionic self-energy on the Matsubara axis $\text{Im}[\Sigma_{\text{loc}}(i\omega_n)]$ for several hole doping levels. We show data for fixed $(U_0, V) = (0.7, 0.3)\text{eV}$, and $T = 40\text{K}$.

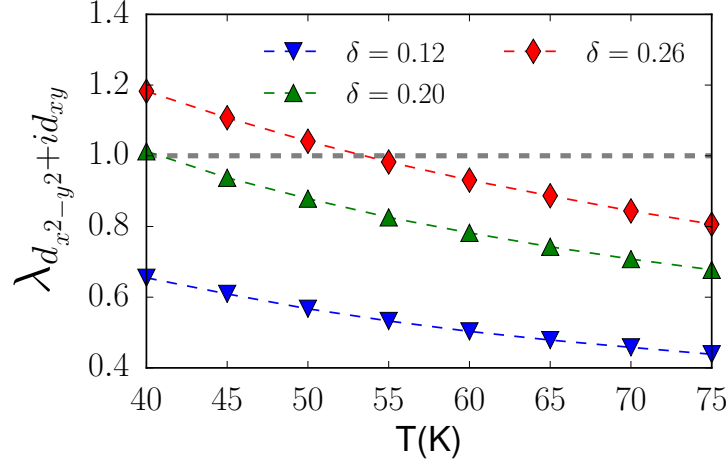


FIG. 7: Plot of λ as a function of temperature T at different doping levels for fixed $U_0 = 0.7\text{eV}$ and $V = 0.3\text{eV}$.

large doping ($\delta \geq 0.5$), in contrast, λ is increased by increasing α (emphasizing the charge channel), which indicates once more that charge fluctuations are key for the emergence of superconductivity at large doping. Finally, for intermediate doping ($\delta \in (0.3, 0.42)$), the largest λ value is found for $\alpha = 0.5$, indicating that in this region charge- and spin fluctuations contribute “cumulatively” to the SC instability. While it is hard to further disentangle the cross influence of charge and spin fluctuations in the self-consistent solution, the insights from the α dependence support the picture of a cooperative (or additive) spin-charge pairing mechanism as discussed in the main text.

Appendix G: Long-range versus short-range non-local interaction

We now show that it is not possible to obtain the same phase diagram (in particular the superconducting phase) with non-local but short-range (e.g. nearest-neighbor) interaction. In Fig. 10(a) we show λ as a function of V for the short-range (diamonds) and long-range (circles) interaction. Please note that V denotes the strength of the $1/r$ tail when long-range interactions are considered while it represents nearest-neighbor interactions only for the short-range version. We not only observe a downturn of λ upon increasing V but, most importantly, a dramatic increase in the associated charge response functions indicating a second order phase transition to a charge ordered phase (Fig. 10(b)). Hence, when only nearest-neighbor interaction is considered, a charge order instability will occur long before superconducting fluctuations become sizable. In the case of true long-range interactions, the situation is quite

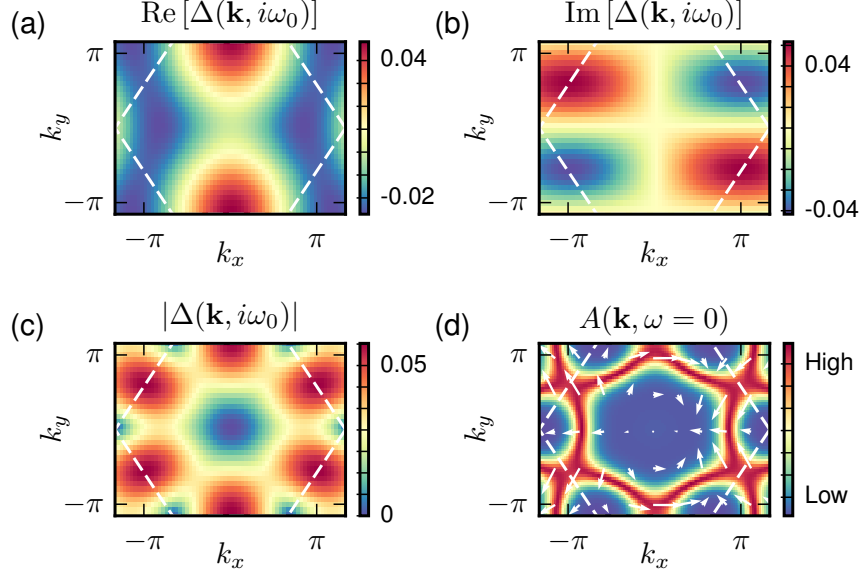


FIG. 8: Momentum dependence of the gap function $\Delta_{d+id'}(\mathbf{k}, i\omega_n)$ at $\omega_n = i\pi T$. (a) $\text{Re}[\Delta_{d+id'}]$, (b) $\text{Im}[\Delta_{d+id'}]$ and (c) $\|\Delta_{d+id'}\|$. (d) Plot of the complex gap function as vectors ($\text{Re}[\Delta_{d+id'}], \text{Im}[\Delta_{d+id'}]$) on top of the momentum dependent spectral function $A(\mathbf{k}, \omega = 0) = -G(\mathbf{k}, \tau = \beta/2)/\pi$. The gap function and spectral function were calculated for $T = 40\text{K}$, $\delta = 0.2$ and $(U_0, V) = (0.7, 0.3)\text{eV}$.

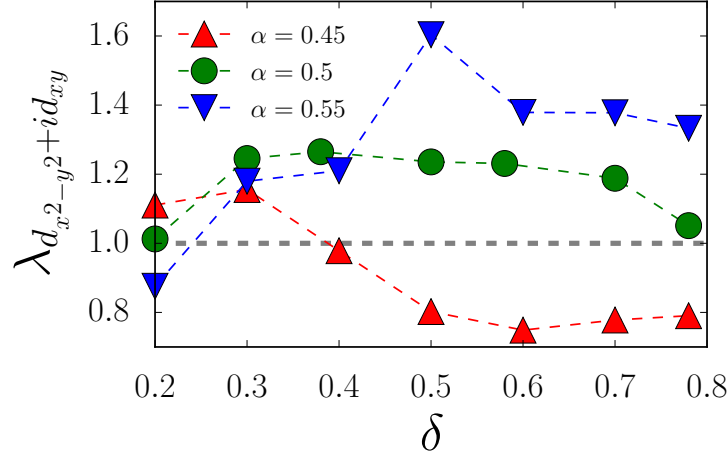


FIG. 9: Chiral d -wave λ values corresponding to different values of the Fierz parameter α as a function of doping. The shown data was obtained at $T = 40\text{K}$, $U_0 = 0.7\text{eV}$, and $V = 0.3\text{eV}$.

different and charge (and spin) fluctuations are enhanced but remain finite up to the point of $\lambda = 1$.

Appendix H: Comparison to the square lattice

As discussed in the main text, the charge/spin pairing mechanism of our chiral SC instability depends crucially on the degeneracy of the $d_{x^2-y^2}$ - and d_{xy} pairing state. This is the case for the triangular lattice where both states belong to the same irreducible representation (E_2). For different lattice geometries where $d_{x^2-y^2}$ - and d_{xy} pairing states are not degenerate the interplay between charge- and spin fluctuation for the SC instability can be qualitatively different from our model. As an important example we mention the 2D square lattice for which $d_{x^2-y^2}$ - and d_{xy} belong

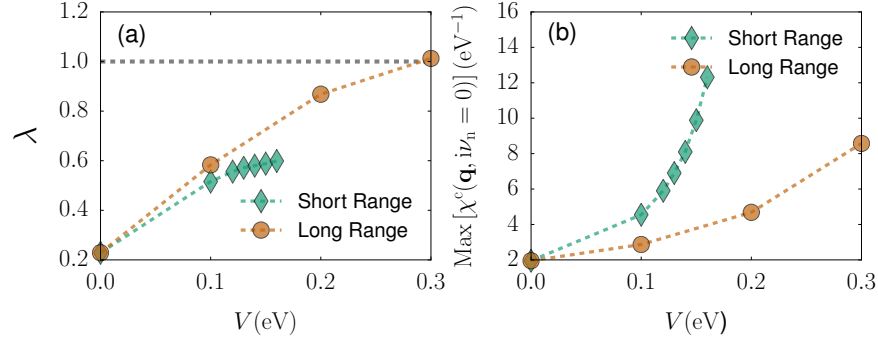


FIG. 10: Comparison of short- and long-range interaction. Here V represents the nearest-neighbor interaction for short-range interaction and the $1/r$ prefactor for long-range interaction. (a) λ values as a function of V for short- (diamond) and long-range interaction (circle). (b) Maximum of static charge susceptibility as a function of V . The parameters are $U_0 = 0.7\text{eV}$, $T = 40\text{K}$ and $\delta = 0.2$.

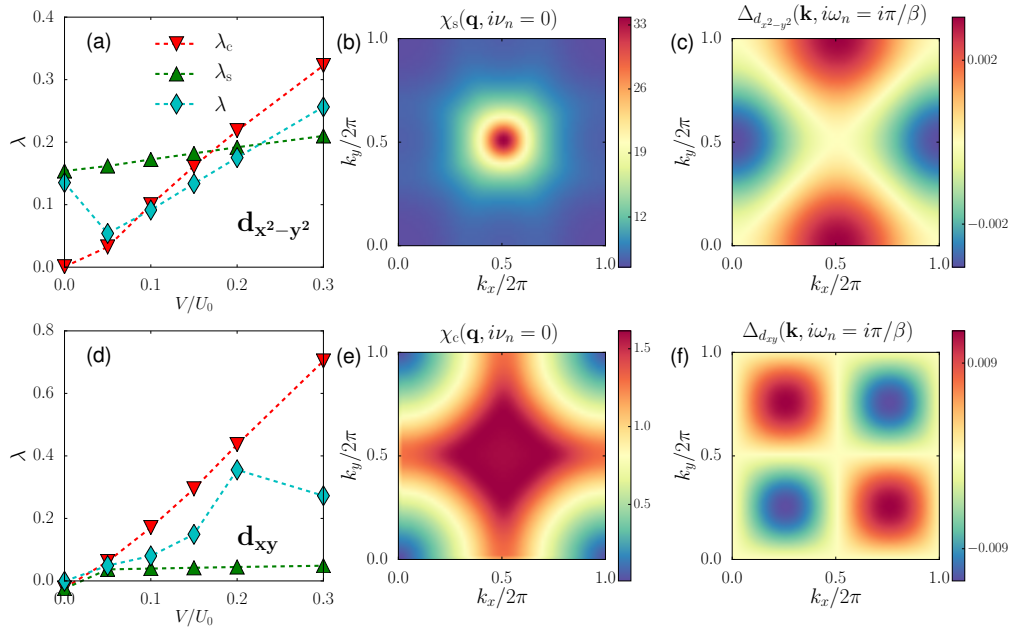


FIG. 11: Simplified TRILEX results for the square lattice with long-range interaction. The parameters are chosen as $t = -0.25\text{eV}$ and $t' = -0.2t$ corresponding to nearest-neighbor and next-nearest-neighbor hopping integrals, on-site interaction $U_0 = 2.0\text{eV}$ and fixed temperature $T = 290\text{K}$. Upper panel: (a) λ values for $d_{x^2-y^2}$ pairing symmetry as a function of long-range interaction strength V computed with charge(down triangular), spin(up triangular) and combined(diamond) contributions; (b) static spin response function; (c) solved $d_{x^2-y^2}$ gap function at $i\omega_n = i\pi/\beta$. Here hole doping level is $\delta = 0.2$, and $V = 0.0\text{eV}$ for (b) and (c). Lower panel: (d) λ values for d_{xy} pairing symmetry as function of long-range interaction strength V computed with charge(down triangular), spin(up triangular) and combined(diamond) contributions; (e) static charge response function; (f) solved d_{xy} gap function. Hole doping level is fixed at $\delta = 0.5$ and $V = 0.6\text{eV}$ for (e) and (f).

to different irreducible representations B_1 and B_2 , respectively. In Fig. 11(a) and (d) we show the corresponding λ values obtained in the square lattice as a function of the long-range interaction V for both $d_{x^2-y^2}$ - and d_{xy} pairing symmetries. With the same separation of channel contribution as performed in the main text, we see a qualitative difference in the behavior of λ : on the triangular lattice, λ is larger than λ_c and λ_s , while on square lattice λ is in between or smaller than λ_c and λ_s .

In order to disentangle the singlet-pairing interaction in the particle-particle channel into charge- and spin contributions we use

$$V^{\text{eff}}(\mathbf{q}, i\nu_n) = W^c(\mathbf{q}, i\nu_n) - 3W^s(\mathbf{q}, i\nu_n) = \frac{U^c(\mathbf{q})}{1 - U^c(\mathbf{q})P^c(\mathbf{q}, i\nu_n)} - 3\frac{U^s}{1 - U^sP^s(\mathbf{q}, i\nu_n)} \quad (\text{H1})$$

$$= U(\mathbf{q}) + \underbrace{\frac{U^c(\mathbf{q})P^c(\mathbf{q}, i\nu_n)U^c(\mathbf{q})}{1 - U^c(\mathbf{q})P^c(\mathbf{q}, i\nu_n)}}_{\text{charge, -}} - 3 \underbrace{\frac{U^s P^s(\mathbf{q}, i\nu_n)U^s}{1 - U^s P^s(\mathbf{q}, i\nu_n)}}_{\text{spin, +}},$$

with $U^c(\mathbf{q}) = \frac{U_0}{2} + v(\mathbf{q})$. The $+(-)$ denotes the positive/negative contribution from each channel ($P^{c/s} < 0$ in our parameter range). We denote the typical pairing-scattering momentum for charge- and spin channel as Q_c (Fig. 11(e)) and Q_s (Fig. 11(b)) respectively (i.e. momenta where $\chi_{c/s}$ are maximal). In order to find a large λ value when solving Eq. (3) $\Delta(\mathbf{k}, i\omega_n)$ should not change sign for scattering with Q_c in the charge channel, while it should change sign when scattering with Q_s . Hence, when spin fluctuations dominate, the $d_{x^2-y^2}$ (Fig. 11(c)) pairing symmetry is favorable in the d -wave singlet pairing and charge fluctuations contribute destructively. Vice versa, when charge fluctuations dominate, d_{xy} (Fig. 11(f)) symmetry will be the favored.
